Influence of Ag and Co additions on glass-forming ability, thermal and mechanical properties of Cu-Zr-Al bulk metallic glasses

B. Escher[1,*], U. Kühn[1], J. Eckert[1,2+], C. Rentenberger[3] and S. Pauly[1,*]

[1]IFW Dresden, Institute for Complex Materials, P.O. Box 27 01 16, D-01171 Dresden, Germany

[2]TU Dresden, Institute of Materials Science, D-01062 Dresden, Germany

[3]University of Vienna, Faculty of Physics, Boltzmanngasse 5, A-1090 Wien, Austria

*corresponding authors: b.escher@ifw-dresden.de, s.pauly@ifw-dresden.de

[+]Present address: Erich Schmid Institute of Materials Science, Austrian Academy of Sciences (ÖAW) and Department Materials Physics, Montanuniversität Leoben, Jahnstraße 12, A-8700 Leoben, Austria

Cite as:

Mat. Sci. Eng. A **673** (2016) 90-98

http://dx.doi.org/10.1016/j.msea.2016.06.081

Abstract

In this study, the effect different amounts of Ag and Co have on thermal stability, phase formation and mechanical properties of the glass-forming alloys $(Cu_{0.5}Zr_{0.5})_{95-x-y}Al_5Ag_xCo_y$ ($2 \leq x \leq 5$ and $0 \leq y \leq 2$) and $Cu_{47.5-y}Zr_{47.5}Al_5Co_y$ ($0 \leq y \leq 2$) was investigated, respectively. The addition of Ag increases the glass-forming ability (GFA) of the alloys by enhancing the stability of the undercooled melt and by simultaneously reducing the stability of the B2 CuZr high-temperature phase. Co instead, has the opposite effect. It leads to an increased thermal stability of the B2 phase, as well as a decreased stability of the undercooled melt and, consequently, lowers the GFA of the alloys. Moreover, a metastable big cube phase precipitates in some alloys stabilized by oxygen, which is introduced during casting. There is a strong interdependence between the phase formation and the tendency of the present alloys to vitrify. This correlation can be captured by the K-parameter (Song et al. 2011 [1]) calculated from the respective transformation temperatures. The plastic strain of the present ternary, quaternary and quinary alloys reflects the GFA as well: the higher the tendency to form a glass, the smaller the plastic strain. Once B2 crystals precipitate in the glass, the plasticity is enhanced significantly.

Keywords: amorphous materials; metallic glasses; mechanical properties; calorimetry; X-ray diffraction

1 Introduction

Bulk metallic glasses (BMGs) are a relative young class of materials [2-4]. They show many unusual properties, especially when compared to their crystalline counterparts. For instance, they have a comparatively low Young's modulus and a large elastic limit [4]. Combined with yield strengths, which approach the theoretical limit, metallic glasses have the capability to store a rather large amount of elastic energy, i.e. they exhibit a large resilience [2, 4]. Their high hardness results in an improved wear resistance [3] and above their glass transition temperature (T_g) metallic glasses can be thermoplastically formed and near-net-shaping becomes feasible [4]. The major drawback, however, is the intrinsic macroscopic brittleness of monolithic metallic glasses due to the autocatalytic strain localization in shear bands [3, 4]. At the early stages of plastic deformation the irreversible strain is solely accommodated in so-called shear transformation zones that percolate and eventually form a shear band, which inevitably leads to fracture on further deformation [5]. To circumvent the limited ductility of bulk metallic glasses, composites consisting of ductile crystals embedded in a glassy matrix have been developed. The crystals hinder the formation and propagation of shear bands and thus can prevent premature failure [3, 5, 6]. The crystalline phase can precipitate in situ in the glassy matrix during casting, for example, when the composition and the cooling conditions are chosen properly [6]. Especially those bulk metallic glass matrix composites have been subject to intense research, in which the crystalline phase exhibits a shape-memory effect [1, 7-10]. One family of these alloys is derived from the binary $Cu_{50}Zr_{50}$ alloy [11, 12]. These shape-memory bulk metallic glass matrix composites show an enhanced damage tolerance and next to an improved plastic strain they exhibit work hardening [7-10].

In order to understand and improve the evolution of the composite microstructures and with it the resulting mechanical properties, it is important to identify and understand the impact of additional alloying elements. Next to the casting parameters, the microstructure evolution upon quenching is mainly influenced by the composition of the alloy [2, 4, 6]. In the case of CuZr-based alloys, certain alloying elements like Al [13-15] and Ag [16, 17], or even both [18-21] increase the glass-forming ability (GFA). The GFA enhancement has been explained by the topological stabilization of atomic clusters in the glass (increase in packing density) due to differing atomic sizes [2]. But more recent ab initio simulations have shown that only Ag decreases the packing density of the cluster, whereas Al, instead, increases it [22]. The enhanced stability of the clusters in CuZr has thus been attributed to the electronic stabilization of the glass by Al or Ag [22].

However, the constituent elements of the alloy also affect the stability of the crystalline phases, which form in these alloy systems. One example is the role Co plays with regard to the thermal stability of the B2 CuZr shape-memory phase, which is only thermodynamically stable at elevated temperatures [23-25]. When a binary CuZr melt is cooled, the B2 phase precipitates at temperatures below 1208 K and if the system is given enough time to equilibrate, it decomposes into the thermodynamically stable $Cu_{10}Zr_7$ and $CuZr_2$ compounds below 988 K [26]. The addition of Co is known to enhance the stability of the B2 CuZr phase significantly [8, 23, 24, 27]. This might be due to the fact that B2 CoZr is stable even at room temperature [28, 29]. Both B2 phases have similar lattice constants (CuZr: 0.3259 nm [25], CoZr: 0.3197 nm [29]) and 5 at.% Co are sufficient to alter the crystallisation sequence on heating in Cu-Zr-Co glasses by stabilizing the B2 phase [23, 24]. At a Co content of at least 10 at.% 3 mm rods solely contain the B2 (Cu,Co)Zr phase [24]. If the CuZr-base alloy is a good glass-former, e.g. $Cu_{46}Zr_{46}Al_8$,

even rods with a diameter of up to 2 mm vitrify after the addition of 4 at.% Co [30]. These reports indicate that CuZr-based glass-formers react quite sensitively to the addition of Al, Ag and Co. To quantify the tendency of a CuZr-based glass-former to form a shape-memory BMG composite, the K-parameter has been introduced [1]. It captures the competition between vitrification, formation of the B2 phase and the low-temperature equilibrium phases ($Cu_{10}Zr_7$ and $CuZr_2$) [1]. Next to the phase formation also the mechanical properties are strongly affected by these alloying elements [8, 13, 14, 16-21, 31-33]. The interrelation between alloy composition, phase selection and mechanical properties is an important aspect to be understood if such materials shall be used in applications in the future.

The aim of this study hence is to simultaneously add Ag as well as Co to a $Cu_{47.5}Zr_{47.5}Al_5$ glass-forming alloy and to investigate (i) how the GFA depends on the stability of the B2 phase and (ii) whether the effects of Co and Ag add or rather compensate each other. Furthermore, the relationship between the GFA and the mechanical properties as well as the impact of B2 crystals on improving the plasticity is addressed.

2 Material and methods

Ingots of the master alloys with a weight of 25 g were prepared by arc melting of high-purity elements (Al, Cu: 99.99 wt.%, Ag, Co: 99.9 wt.% Zr: 99.8 wt.%) under a Ti-gettered Ar atmosphere. The selected compositions cover $(Cu_{0.5}Zr_{0.5})_{95-x-y}Al_5Ag_xCo_y$ (x = 0, 2, 5 and y = 0, 0.5, 1, 2) and are indicated in the pseudo-ternary phase diagram in Fig. 1. The ingots were re-melted at least three times and their actual composition was controlled by inductively-coupled plasma optical emission spectroscopy (ICP-OES, Thermo Scientific IRIS Intrepid II XUV and iCAP 6000). For $Cu_{46.5}Zr_{47.5}Al_5Co_1$, $Cu_{45.5}Zr_{47.5}Al_5Co_2$ and

$Cu_{45.5}Zr_{45.5}Al_5Ag_2Co_2$ (alloys 3, 4, and 8, Table 2; 3 and 8 also marked by stars in Fig. 1), rods and ribbons were investigated by ICP-OES and the oxygen content was measured by thermal extraction with a carrier gas (LECO, TC436DR). Rods with a diameter of 2 mm were cast with a suction-casting device (Bühler MAM1). Additionally, ribbons were produced by means of a single-roller melt spinner (Edmund Bühler GmbH) using a BN-coated SiO_2 nozzle. The alloys were ejected about 200 K above their respective liquidus temperature.

Thermal analysis was conducted in a high-temperature differential scanning calorimeter (Netzsch DSC 404 C) and in a conventional DSC (Perkin-Elmer Diamond). For the Netzsch DSC 404 C a heating and cooling rate of 20 K/min and alumina crucibles were used up to a temperature of 1423 K. The measurements in the Perkin-Elmer Diamond DSC were done using Al crucibles at heating rates ranging from 5 K/min to 300 K/min from a temperature of 313 K to 863 K. The calorimetric glass transition temperatures T_g (half c_p) and the crystallization temperatures T_x (onset) were obtained from low-temperature DSC measurements.Additionally, start and end of the eutectoid transformation (T_s) and (T_f), the solidus temperature T_{sol} and the liquidus temperature T_{liq} determined by the high-temperature measurements of 2 mm rods. The results from the ribbons (DSC Diamond) were used to calculate the activation energy of crystallisation [34]. A STOE STADI P XRD device with Mo-Kα_1 radiation (λ_1 = 0.070932 nm) was used for structural characterization in transmission mode.

The compression tests were conducted using samples with a diameter of 2 mm and a length of 4 mm in an Instron 5869 applying a displacement rate of 4 x 10^{-4} mm/s. The sample faces were lubricated with “Molykote” (Dow Corning Corporation) and WC-Co hard metal plates were placed between the samples and the compression plungers. At

least three samples of each composition were tested. The strain was determined with a laser extensometer (Fiedler Optoelectronics GmbH). The elastic constants were measured with the help of an Olympus Panametrics-NDT 5900PR ultrasonic device.

The amount of B2-phase in the compression samples was determined from optical micrographs (Zeiss Axiophot microscope, Carl Zeiss AG) of the upper and lower cross section of each sample, averaged over 3-6 rods and additionally by calorimetric measurements based on the respective crystallisation enthalpies of the ribbons and rods.

3 Results and discussion

Table 1 lists the nominal composition of the present alloys and the compositions of the different ingots obtained from ICP-OES. Both values show an excellent agreement within the experimental error. The only exception is a slightly lower actual Co content (1.86 at.%) in $Cu_{45.5}Zr_{45.5}Al_5Ag_2Co_2$ (alloy no. 8).

The following discussion focuses on two main aspects. The first part deals with the thermal properties of the alloys and the influence of Ag and Co on the characteristic transformation temperatures and the phase formation. Moreover, parameters are calculated from these temperatures, which have been reported to indicate the GFA or the tendency of an alloy to solidify into composite microstructures. In the second part we address the elastic and plastic deformation and correlate it with the glass-forming ability and the content of shape-memory crystals.

3.1 Thermal properties and phase formation

Fig. 2 shows the high-temperature DSC traces of two selected alloys, in order to illustrate the influence of composition on the relevant characteristic temperatures (gained from

2 mm rods), which are the glass transition temperature (T_g), the crystallization temperature (T_x), start and end of the eutectoid transformation (T_s) and (T_f), the solidus temperature T_{sol} and the liquidus temperature T_{liq}.

In addition, differences in the crystallisation behaviour between ribbons and rods are observed. While the ribbons of the compositions marked by a star in Fig. 1 show a splitting of the crystallisation peak, the rod samples only exhibit one major exothermic event (Fig. 3a). There is also a shift of the onset of crystallization to higher temperatures in the case of ribbons. The XRD patterns of $Cu_{46.5}Zr_{47.5}Al_5Co_1$ (alloy no. 3, Fig. 3b) and $Cu_{45.5}Zr_{45.5}Al_5Ag_2Co_2$ (alloy no. 8, Fig. 3c) ribbons heated to a temperature in between these two crystallisation peaks indicate the characteristic peaks of the metastable “big cube” phase [35, 36]. After the second exothermic peak the “big cube” phase has completely transformed into the low-temperature equilibrium phases $Cu_{10}Zr_7$ and $CuZr_2$ [26]. These two phases are also detected in $Cu_{45.5}Zr_{47.5}Al_5Co_2$ (alloy no. 4) after complete crystallization. $Cu_{45.5}Zr_{47.5}Al_5Co_2$ is an alloy for which the crystallization sequence in the rod and the ribbon is identical. Crystallization occurs in one exothermic event and the respective diffraction pattern is added to both diagrams for comparison.

Since oxygen is known to stabilize the “big cube” phase [36, 37], which has a pronounced icosahedral coordination [35, 36, 38], special attention was paid to the oxygen content in the alloys.

As Table 2 indicates, the oxygen content measured for $Cu_{46.5}Zr_{47.5}Al_5Co_1$ (alloy no. 3) and $Cu_{45.5}Zr_{45.5}Al_5Ag_2Co_2$ (alloy no. 8) ribbons exceeds 11000 ppm, whereas the oxygen level is about 2000 ppm in the case of $Cu_{45.5}Zr_{47.5}Al_5Co_2$ (alloy no.4) ribbons. This rather high oxygen content in alloys 3 and 8 must be the reason for the “big cube” formation. There is a systematic enrichment in oxygen in the melt-spun ribbons compared to the rods

(oxygen content about 250 ppm). Since the ribbons and the rods were prepared from the same ingots, this discrepancy is caused by the preparation method. Apparently, the melt reacted with the quartz crucible during melt spinning and oxygen as well as silicon were dissolved in the alloy. It could be that the alloy melt was overheated too much and that the melt was kept at this temperature for too long [39].

The values of T_g, T_x, T_f and T_{liq} of rods with a diameter of 2 mm are given in Table 3 for all compositions. The glass transition temperature and the crystallization temperature vary within 10 K. These almost constant values reflect the only small compositional changes and a similar effect has been reported for Ag-containing CuZr-based alloys, for instance [16, 19, 20]. In contrast, T_s and T_f as well as T_{sol} and T_{liq} are much more composition-dependent. T_f and T_{sol} are plotted in Fig. 4 as a function of the Ag content. When the amount of Ag reaches about 5 at.%, Tsol decreases by about 65 K. In contrast, Tf increases by about 80 K until it eventually merges with the endothermic melting signal (Tsol) for Cu45Zr45Al5Ag5 (alloy no. 9) (Fig. 2). The behaviour of T_f and T_{sol} is in good agreement with what has been observed for similar alloys [1, 16, 17, 19-21] and suggests that the B2 phase is less prone to form in alloys with a large Ag content. Co, on the contrary, leads to an increase of T_{sol} and lowers T_f. In other words, the temperature regime, in which the B2 phase is stable, becomes larger. This stabilization of the B2 phase by Co has been also reported for $Cu_{50-x}Zr_{50}Co_x$ [24], $(Cu_{0.5}Zr_{0.5})_{100-x}Co_x$ [23] and $(Cu_{0.5}Zr_{0.5})_{90-x}Al_{10}Co_x$ [1]. Fig. 4 also indicates that the addition of Ag to the present Cu-Zr-Al-Co alloys diminishes the influence Co has on extending the temperature window, in which the B2 phase can be found. Both elements Co and Ag can thus be efficiently used to adjust the thermal stability of the B2 phase, which is the crystalline phase competing with vitrification on rapid cooling [40, 41].

These findings help to explain the diffraction results of the 2 mm rods shown in Fig. 5. B2 (Cu,Co)Zr reflections were only found in the case of $Cu_{45.5}Zr_{47.5}Al_5Co_2$ (no. 4) and $Cu_{45.5}Zr_{45.5}Al_5Ag_2Co_2$ (alloy no. 8) for which the interval between T_{sol} and T_f is relatively large. When 2 at.% Co are added to $Cu_{45}Zr_{45}Al_5Ag_5$ (alloy no. 9) the diffraction patterns suggest that the alloy is quenched into a fully glassy state (Fig. 5c) because the stability region of the B2 phase is relatively small. The glass-forming ability in these alloys thus appears to be directly related to the stability of the B2 (Cu,Co)Zr phase, and Ag enhances the tendency of the alloys to vitrify and Co reduces it. Yet, it is noteworthy that the temperature interval $T_{sol} - T_f$ alone is not sufficient to predict whether an alloy forms a glass or a composite at a given cooling rate. The $Cu_{46.5}Zr_{47.5}Al_5Co_1$ (alloy no. 3) rods, for instance, cast into fully amorphous samples according to the X-ray diffraction patterns ($T_{sol} - T_f = 181 \pm 3$ K), while the $Cu_{45.5}Zr_{45.5}Al_5Ag_2Co_2$ (no. 8) rods with the same dimensions contain B2 crystals ($T_{sol} - T_f = 117 \pm 3$ K).

When B2 crystals precipitate in the glassy matrix, their distribution is very heterogeneous with few relatively large (~ 100 µm) crystals being present in the glassy matrix (see Fig. 6). Such a microstructure is commonly observed in these composites [1, 7, 9]. Due to the heterogeneous distribution of crystals, it is difficult to deduce reliable crystalline volume fractions from XRD patterns. This holds true also for the B2 contents determined from optical microscopy (OM) and calorimetric measurements and results in the relatively large scattering of the determined volume fractions (Table 4). Even though the heterogeneous morphology of the composites aggravates an exact determination of volume fractions, the overall trend is consistent: the higher the Ag content in the alloys, the higher the critical diameter (GFA). An increasing Co content, however, leads to an enhanced volume fraction of B2 phase crystallites embedded in the glassy matrix.

To describe the tendency of a CuZr-based alloy to form a BMG composite, the K-parameter has been proposed [1]. It is based on the competition between the formation of the low-temperature equilibrium phases and the formation of the B2 phase on one side and the stability of the liquid on the other side. The K-parameter is given by [1]:

$$K = \frac{T_f}{T_{liq}} \qquad (1)$$

The higher the value of K, the stronger is the bias of an alloy towards forming a glass at a given cooling rate.

Additionally, to assess the glass-forming ability alone in the investigated alloys, we also calculated their γ-parameters [42]:

$$\gamma \propto \frac{T_x}{T_g + T_{liq}} \qquad (2)$$

The higher the value of γ, the higher the GFA of an alloy generally is. The calculated values of γ and K are listed in Table 3 and are plotted in Fig. 7. Both parameters show the same trends: they increase when more Ag is present in the alloy and the addition of Co (at a fixed Ag content) reduces them. These results again indicate that Ag increases the glass-forming ability and that Co has the opposite effect. Except for the alloy containing 5 at.% Ag all values of the K-parameter are within the region of the "type II" alloys [1]. They are characterized by the B2 transformation proceeding between the crystallization of $Cu_{10}Zr_7$ and $CuZr_2$ from the glass, and the melting. This means, that they still show significant GFA, because the B2 phase is not stable at low temperatures. So, in a highly undercooled melt (T < 988 K) the thermodynamic stability of $Cu_{10}Zr_7$ and $CuZr_2$ is higher than for the B2 phase [26]. However, because the eutectic precipitation of $Cu_{10}Zr_7$ and $CuZr_2$ from an undercooled melt is diffusion-controlled [43], it can be kinetically suppressed by a high cooling rate and thus a glass is able to form. However, the B2 phase in "type II" alloys is stabilized below T_{sol}, so that it may precipitate from the melt on cooling.

The K values gained for the base alloy $Cu_{47.5}Zr_{47.5}Al_5$ (K = 0.891) [1] differ from the ones within this work ($K = 0.836 \pm 2 \times 10^{-4}$). This deviation might be due to different

determination of the characteristic temperatures from the DSC traces. Song et al. [1] used the end of a small endothermic signal after the main transformation peak (1055 ± 2 K) to determine T_f, whereas we used the end of the peak (991 ± 2 K) in the present work instead.

The GFA is also reported to be connected to the activation energies of crystallization (E_a) [44-46]. The lower the activation energies of crystallization (E_a) are, the less stable the glass is against crystallization and thus the GFA is expected to be lower as well [44-46]. Even though this method determines the energy needed to activate crystallization on heating of a glass and one has to be careful because of the "asymmetric" phase formation on heating and cooling, we wanted to explore if there is a link between the phase formation (GFA) and E_a. Furthermore, for the ribbons precipitating the "big cube" phase it is proposed, that E_a should be lower than for the low-temperature equilibrium phases [47]. This is based on the assumption, that the structural similarity between the glass, with a high fraction of icosahedral order, and the icosahedral "big cube" phase leads to a low E_a. Additionally, a correlation between the plasticity and E_a in different binary CuZr alloys was reported [48]. With rising E_a the alloys exhibit a decrease in plasticity. This relationship is addressed in the next section dealing with the mechanical properties. The activation energies of crystallization are given in Table 3 and are also depicted in Fig. 8. E_a = 407 ± 10 kJ/mol for $Cu_{47.5}Zr_{47.5}Al_5$ and gradually decreases to about 325 ± 13 kJ/mol for $Cu_{45}Zr_{45}Al_5Ag_5$ with the addition of Ag. Co generally seems to decrease the activation energy of crystallization as well. If one assumes that a lower E_a is associated with a lower GFA [44-46], the alloys should become worse glass formers with increasing Ag and Co content. This conclusion, however, contradicts the trends revealed for the γ- and K-parameter (Fig. 7) and what has been reported elsewhere [17-21, 49]. So, the GFA does

not appear to be correlated with E_a in the present alloys. The “asymmetric” phase formation on heating and cooling might be the reason for these discrepancies and contradictions [44-46].

The behaviour of E_a becomes rather complex when the “big cube” phase forms. The activation energies for the first crystallization event in which the “big cube” phase forms (E_{a1}) and of the second crystallization process (formation of the low-temperature equilibrium phases, $Cu_{10}Zr_7$ and $CuZr_2$, E_{a2}) were calculated. The respective activation energies of crystallization are given in Table 3 and Fig. 8 (marked by stars) for the alloys $Cu_{46.5}Zr_{47.5}Al_5Co_1$ (alloy no. 3), $Cu_{45.5}Zr_{45.5}Al_5Ag_2Co_2$ (alloy no. 8) and $Cu_{45}Zr_{45}Al_5Ag_5Co_2$ (alloy no. 10). One finds that E_{a1} is always lower than E_{a2}, as proposed in [47]. However, a much lower E_{a1} compared to the energy required to precipitate the equilibrium phases ($Cu_{10}Zr_7$ and $CuZr_2$) [47], is not suggested by our results. The activation energies for the other alloys are equal to the ones for the formation of the “big cube” phase.

3.2 Mechanical properties

In the following paragraphs, the emphasis is placed on the differences in the mechanical properties between the various BMGs and the BMG matrix composites and the respective influence Ag and Co have on them. We determined the yield strength (R_p), the plastic strain (ε_p) and the Young’s modulus (E_c) from compression tests. Additionally the Young’s modulus (E_{US}) and the Poisson’s ratio (ν_{US}) were measured by means of ultrasound velocities (Table 4).

Two selected stress-strain curves for each alloy are displayed in Fig. 9. The crystalline volume fractions as determined from the optical analysis are indicated. All samples exhibit high yield strengths above 1700 MPa and plastic strains between 0% and 7%. No

apparent work hardening is observed in the present glasses or composites, contrary to what has been reported for a $Cu_{47.5}Zr_{47.5}Al_5$ glass [14]. Interestingly, also the BMG composites lack work hardening, but this must be due to the low crystalline volume fractions (below 5 vol.%). Such a small amount of crystals cannot overcompensate the work softening of the glassy matrix [7, 40]. At the same time, the low crystalline volume fraction has virtually no impact on the yield strength, which is constant within the experimental error, regardless of the volume fraction or composition. Generally, if a crystalline phase is embedded in a glassy matrix it has a pronounced impact on the yield strength of the glass [3-8]. But in the case of CuZr-based BMG composites, the yield strength should be only lowered drastically when the B2 CuZr volume fraction exceeds about 10 vol.% [7, 40]. As opposed to the yield strength, the plasticity of BMGs can react quite sensitively even to minor changes in the composition [13, 14, 16, 31, 32, 49] and also the presence of a relatively small amount of B2 CuZr crystals can enhance the plastic strain significantly [7, 40].

The influence of the composition on the plasticity of the glasses as well as the effect of the B2 crystals on the deformability of the composites shall now be addressed. It is important to note here, that the plastic strain has an intrinsic scattering and that the determination of the crystalline volume fractions by optical methods is not very accurate due to the heterogeneous distribution of the crystals. In order to account for this scattering in the plastic strain, the curves with the smallest and largest plastic strain are shown for each alloy in the Fig. 9a-c. Whereas the plastic strains of all tested samples are used for the calculation of the values in Table 4. As stated above, when Ag is added to the Cu-Zr-Al alloy, its glass-forming ability increases. This is accompanied by a lower plasticity (Fig. 9a and Table 4). This corresponds well with reports of similar compositions

containing various amounts of Ag [16, 18, 20, 32]. However, the plasticity is significantly less than reported for $Cu_{43}Zr_{43}Al_7Ag_7$ [33] and $Cu_{40}Zr_{45}Al_7Ag_8$ [21]. At such high Al and Ag contents phase separation occurs [33] and this has been accounted for the large plastic strain of 9% in compression [5, 33].

The effect of Co on the plasticity of the glass can be illustrated by comparing the stress-strain curves for different amounts of Ag. When no Ag is present in the alloy (i.e. $Cu_{47.5}Zr_{47.5}Al_5$ – no. 1), the addition of Co (e.g. $Cu_{45.5}Zr_{47.5}Al_5Co_2$ – no. 4) results in the precipitation of an elevated amount of B2 shape-memory crystals and a marginal increase in plasticity (Fig. 9a, Table 4). The alloys based on $Cu_{46.5}Zr_{46.5}Al_5Ag_2$ show similar plasticity up to 1 at.% Co (Fig. 9b). For $Cu_{45.5}Zr_{45.5}Al_5Ag_2Co_2$ (no. 8), plasticity as well as the B2 content are increased. In the case 2 at.% Co (no. 10) are added to $Cu_{45}Zr_{45}Al_5Ag_5$ (no. 9) (ε_p = 1.1 ± 1.2 %), the rod with a diameter of 2 mm remains glassy but the plastic strain is slightly raised (ε_p = 2.4 ± 0.7 %) (Fig. 9b).

The small volume fractions of the large B2 crystals and their heterogeneous distribution are one reason for the ambiguous trends of the plasticity with the compositional changes. The overall trends are nevertheless observable: High contents of Ag lead to enhanced GFA and thus to reduced plasticity [16, 18, 20, 32]. Large contents of Co decrease the GFA, lead to precipitation of B2 crystallites in the glassy matrix and thus tend to enhance the plasticity [7]. For equal amounts of Ag and Co in the alloy (within the limits given in this study), the effects of the elements seem to compensate each other and the plasticity remains constant.

Comparing the trends of the activation energy of crystallization (E_a) (Table 3 and Fig. 7) with the ones for the plasticity of the different alloys, the opposite of what has been proposed previously [48] can be identified. Our results show, that an increase in the Ag

content leads to a decreasing E_a, as well as to a reduced plasticity. So the proposed correlation is apparently not universal and not applicable for the alloys studied here.

The flow of all investigated samples in the plastic regime is characterized by serrations. They indicate the heterogeneous nature of the deformation via localized shear band sliding and arrest as it is characteristic of BMGs [3-5]. The stress drop amplitudes do not appear to be affected by the presence of such low amounts of crystals [50].

As a last aspect, the elastic constants shall be addressed. The Young's moduli obtained by compression tests and ultrasonic measurements are listed in Table 4. Because the volume fraction of the B2 phase is rather low, the results obtained from glasses and composites are discussed together for simplicity. The Young's modulus (E_{US}) rises linearly from about 87.5 ± 0.7 GPa to about 90.5 ± 0.7 GPa for Ag contents from 0 at.% to 5 at.%. Also for the Young's modulus obtained by compression a rise from 87 ± 5 GPa to 93 ± 3 GPa is observed, similar to previously reported values [16, 20]. Ab initio studies [22] have attributed an enhanced electronic stability of the atomic clusters and thus the atomic bonds for the higher Young's modulus at larger Ag contents. The changes of Young's modulus with increasing Co content are within the experimental error for both methods. However, from the compression test results a slight but steady increase is observed.

The Poisson's ratio, which is a critical parameter for the deformability of BMGs [3, 5, 6], is roughly constant for all investigated compositions.

Conclusions

In terms of glass-forming ability of $Cu_{50}Zr_{50}$-based alloys additions of Co and Ag act as antagonists. Ag and Co both affect the liquidus temperature and the temperature, at which

B2 CuZr decomposes eutectoidly. Both elements hence influence the stability of the crystalline phase, which competes with the formation of a glass. When Co is added to the multicomponent glass-forming alloys, their tendency to vitrify is reduced and instead B2 crystals precipitate in the glassy matrix. Ag, on the other hand, increases the GFA and the compositions containing higher Ag contents show less or no B2 crystals. The GFA is apparently not correlated with the activation energy of crystallization (E_a). A “big cube” phase forms during heating in the melt-spun ribbons of some alloys due to high oxygen contents above 11000 ppm.

The effect of the compositional changes and the volume fraction of the B2 phase on the mechanical properties are difficult to separate. The yield strength and the fracture mechanism are independent of the small volume fraction of the B2 phase as well as the marginal compositional changes investigated in the present work. However, the plasticity follows certain trends: Large contents of Ag lead to reduced plasticity, because of an enhanced glass-forming ability; high contents of Co enhance the plasticity and lead to precipitation of B2 crystallites in the glassy matrix [7]. E_a is not correlated to the plasticity at as might apply when deformation is accompanied by the precipitation of crystals. Furthermore, the Young’s modulus is only slightly raised by increasing Ag contents and not affected by Co and the Poisson’s ratio remains constant.

Altogether, the phase formation of CuZr-base alloys strongly depends on the stability of the competing phases and has a tremendous effect on the mechanical properties. It has been found, that the stability of the phases and thus the mechanical properties can be effectively adjusted with definite amounts of Ag and Co additions.

Acknowledgements

We thank S. Donath for his advice concerning the casting; B. Bartusch and A. Voss for technical assistance; I. Kaban, C. Ebner, C. Gammer, H.P. Karnthaler and K. Kosiba for stimulating discussions. The authors gratefully acknowledge the funding by the German Science Foundation under Grant PA 2275/2-1 and the Austrian Science Fund FWF:[I1309]. This work was also supported by the Leibniz Program (Grant EC 111/26-1), as well as the German Federal Ministry of Education and Research BMBF (Project No. 05K2012). J.E. acknowledges the funding by the ERC Advanced Grant INTELHYB (grant ERC-2013-ADG-340025).

References

[1] K.K. Song, S. Pauly, Y. Zhang, P. Gargarella, R. Li, N.S. Barekar, U. Kühn, M. Stoica, J. Eckert, Acta Mater., 59 (2011) 6620-6630.
[2] A. Inoue, Proc. Jpn. Acad., Ser. B, Phys. Biol. Sci., 81 (2005) 156-171.
[3] M.M. Trexler, N.N. Thadhani, Prog. Mater Sci., 55 (2010) 759-839.
[4] A.L. Greer, Mater. Today, 12 (2009) 14-22.
[5] A.L. Greer, Y.Q. Cheng, E. Ma, Mater. Sci. Eng., R, 74 (2013) 71-132.
[6] J. Eckert, J. Das, S. Pauly, C. Duhamel, J. Mater. Res., 22 (2007) 285-301.
[7] S. Pauly, G. Liu, G. Wang, J. Das, K.B. Kim, U. Kühn, D.H. Kim, J. Eckert, Appl. Phys. Lett., 95 (2009) 101906.
[8] F.F. Wu, K.C. Chan, S.T. Li, G. Wang, J. Mat. Sci., 49 (2014) 2164-2170.
[9] Y. Wu, Y. Xiao, G. Chen, C.T. Liu, Z. Lu, Adv. Mater., 22 (2010) 2770-2773.
[10] P. Gargarella, S. Pauly, K.K. Song, J. Hu, N.S. Barekar, M. Samadi Khoshkhoo, A. Teresiak, H. Wendrock, U. Kühn, C. Ruffing, E. Kerscher, J. Eckert, Acta Mater., 61 (2013) 151-162.
[11] M.W. Chen, A. Inoue, W. Zhang, T. Sakurai, Phys. Rev. Lett., 96 (2006) 245502.
[12] Z.W. Zhu, H.F. Zhang, W.S. Sun, B.Z. Ding, Z.Q. Hu, Scripta Mater., 54 (2006) 1145-1149.
[13] T.A. Baser, J. Das, J. Eckert, M. Baricco, J. Alloys Compd., 483 (2009) 146-149.
[14] J. Das, M.B. Tang, K.B. Kim, R. Theissmann, F. Baier, W.H. Wang, J. Eckert, Phys. Rev. Lett., 94 (2005) 205501.
[15] W.H. Wang, J.J. Lewandowski, A.L. Greer, J. Mater. Res., 20 (2005) 2307-2313.
[16] G. Duan, K. De Blauwe, M.L. Lind, J.P. Schramm, W.L. Johnson, Scripta Mater., 58 (2008) 159-162.
[17] W. Zhang, A. Inoue, J. Mater. Res., 21 (2006) 234-241.

[18] W. Zhang, C.L. Qin, X.G. Zhang, A. Inoue, Mater. Sci. Eng., A, 449 (2007) 631-635.
[19] D.S. Sung, O.J. Kwon, E. Fleury, K.B. Kim, J.C. Lee, D.H. Kim, Y.C. Kim, Met. Mater. Int., 10 (2004) 575-579.
[20] N. Barekar, P. Gargarella, K.K. Song, S. Pauly, U. Kühn, J. Eckert, J. Mater. Res., 26 (2011) 1702-1710.
[21] Q.K. Jiang, X.D. Wang, X.P. Nie, G.Q. Zhang, H. Ma, H.J. Fecht, J. Bednarcik, H. Franz, Y.G. Liu, Q.P. Cao, J.Z. Jiang, Acta Mater., 56 (2008) 1785-1796.
[22] Z.D. Sha, Q.X. Pei, J. Alloys Compd., 619 (2015) 16-19.
[23] K. Kosiba, P. Gargarella, S. Pauly, U. Kuhn, J. Eckert, J. Appl. Phys., 113 (2013) 123505-123504.
[24] F.A. Javid, N. Mattern, S. Pauly, J. Eckert, Metallurgical and Materials Transactions A, 43 (2011) 2631-2636.
[25] E.M. Carvalho, I.R. Harris, J. Mat. Sci., 15 (1980) 1224-1230.
[26] D. Arias, J.P. Abriata, Bull. Alloy Phase Diagr., 11 (1990) 452-459.
[27] S. Pauly, K. Kosiba, P. Gargarella, B. Escher, K.K. Song, G. Wang, U. Kühn, J. Eckert, J. Mater. Sci. Technol., 30 (2014) 584-589.
[28] W.H. Pechin, D.E. Williams, W.L. Larsen, Trans. ASM, 57 (1964) 646.
[29] K.H.J. Buschow, J. Less Common Metals, 85 (1982) 221-231.
[30] W. Zhou, Y. Tao, L. Liu, L. Kong, J. Li, Y. Zhou, Mater. Trans., JIM, 54 (2013) 286-290.
[31] P. Yu, H.Y. Bai, Mater. Sci. Eng., A, 485 (2008) 1-4.
[32] Q.S. Zhang, W. Zhang, A. Inoue, Mater. Trans., JIM, 48 (2007) 1272-1275.
[33] J.C. Oh, T. Ohkubo, Y.C. Kim, E. Fleury, K. Hono, Scripta Mater., 53 (2005) 165-169.
[34] H.E. Kissinger, Anal. Chem., 29 (1957) 1702-1706.
[35] J. Saida, M. Matsushita, A. Inoue, Intermetallics, 10 (2002) 1089-1098.
[36] J. Eckert, N. Mattern, M. Zinkevitch, M. Seidel, Mater. Trans., JIM, 39 (1998) 623-632.
[37] B.S. Murty, D.H. Ping, K. Hono, A. Inoue, Acta Mater., 48 (2000) 3985-3996.
[38] R. Mackay, G.J. Miller, H.F. Franzen, J. Alloys Compd., 204 (1994) 109-118.
[39] Z. Altounian, E. Batalla, J.O. Strom-Olsen, J.L. Walter, J. Appl. Phys., 61 (1987) 149-155.
[40] S. Pauly, G. Liu, G. Wang, U. Kühn, N. Mattern, J. Eckert, Acta Mater., 57 (2009) 5445-5453.
[41] S. Pauly, J. Das, C. Duhamel, J. Eckert, Adv. Eng. Mater., 9 (2007) 487-491.
[42] Z.P. Lu, C.T. Liu, Acta Mater., 50 (2002) 3501-3512.
[43] D.M. Herlach, Mat Sci Eng R, 12 (1994) 225.
[44] F.Q. Guo, S.J. Poon, G.J. Shiflet, Scripta Mater., 43 (2000) 1089-1095.
[45] Z. Sniadecki, U.K. Rössler, B. Idzikowski, Acta Phys. Pol., A, 115 (2009) 409-412.
[46] H.S. Chen, Appl. Phys. Lett., 29 (1976) 12-14.
[47] M.H. Lee, R.T. Ott, M.F. Besser, M.J. Kramer, D.J. Sordelet, Scripta Mater., 55 (2006) 505-508.
[48] J.C. Lee, K.W. Park, K.H. Kim, E. Fleury, B.J. Lee, M. Wakeda, Y. Shibutani, J. Mater. Res., 22 (2007) 3087-3097.
[49] Q.S. Zhang, W. Zhang, A. Inoue, Scripta Mater., 55 (2006) 711-713.

[50] K.K. Song, S. Pauly, B.A. Sun, J. Tan, M. Stoica, U. Kühn, J. Eckert, AIP Advances, 3 (2013) 012116.

Table 1: Nominal and actual chemical compositions of the ingots of all investigated alloys

No.		Cu (at.%) ± 0.2	Zr (at.%) ± 0.2	Al (at.%) ± 0.04	Ag (at.%) ± 0.04	Co (at.%) ± 0.04
1	Nominal	47.50	47.50	5,00	-	-
	ICP-OES	47.66	47.37	4.97	-	-
2	Nominal	47.50	47.00	5.00	-	0.50
	ICP-OES	47.48	46.95	5.12	-	0.44
3	Nominal	46.50	47.50	5.00	-	1.00
	ICP-OES	46.80	47.26	4.96	-	0.98
4	Nominal	45.50	47.50	5.00	-	2.00
	ICP-OES	46.39	46.68	4.92	-	2.00
5	Nominal	46.50	46.50	5.00	2.00	-
	ICP-OES	46.49	46.51	5.01	2.00	-
6	Nominal	46.25	46.25	5.00	2.00	0.50
	ICP-OES	46.23	46.29	4.99	2.00	0.50
7	Nominal	46.00	46.00	5.00	2.00	1.00
	ICP-OES	45.97	46.06	4.98	1.99	1.00
8	Nominal	45.50	45.50	5.00	2.00	2.00
	ICP-OES	45.63	45.52	5.01	1.98	1.86
9	Nominal	45.00	45.00	5.00	5.00	-
	ICP-OES	45.11	44.84	5.04	5.02	-
10	Nominal	44.00	44.00	5.00	5.00	2.00
	ICP-OES	44.16	43.96	5.00	4.88	2.01

Table 2: Nominal and actual compositions of rods and ribbons of $Cu_{46.5}Zr_{47.5}Al_5Co_1$, $Cu_{45.5}Zr_{47.5}Al_5Co_2$ and $Cu_{45.5}Zr_{45.5}Al_5Ag_2Co_2$ (alloys no.3, 4 and 8) including the content of the contaminants oxygen and silicon.

No.		Cu (at.%) ± 0.1	Zr (at.%) ± 0.1	Al (at.%) ± 0.04	Ag (at.%) ± 0.04	Co (at.%) ± 0.04	Si (at.%) ± 0.04	O (ppm)
3	Nominal	46.50	47.50	5.00	-	1.00	-	-
	2 mm rod	46.66	47.27	4.97	-	0.97	0.11	252 ± 8
	Ribbon	45.74	46.29	4.94	0.14	0.98	0.74	11 720 ± 6
4	Nominal	45.50	47.50	5.00	-	2.00	-	-
	2 mm rod	45.60	47.24	4.98	-	2.01	0.13	281 ± 43
	Ribbon	45.50	47.02	5.02	-	2.01	0.24	2197 ± 329
8	Nominal	45.50	45.50	5.00	2.00	2.00	-	-
	2 mm rod	45.68	45.24	5.02	1.99	1.85	0.19	273 ± 10
	Ribbon	44.63	44.25	4.92	1.91	2.38	0.71	11 918 ± 6

Table 3: Characteristic temperatures T_g and T_x (DSC-Diamond - 20 K/min), T_f and T_{liq} (Netzsch DSC 404 C - 20 K/min), the parameters γ and K and activation energy of crystallisation, E_a, for all alloys. Where E_a 1st is calculated from the first crystallisation peak and E_a 2nd from a potential second peak.

No.	Alloy	T_g (K) ± 1 K	T_x (K) ± 1 K	T_f (K) ± 2 K	T_{liq} (K) ± 2 K	γ ± 1 x 10^{-4}	K ± 2 x 10^{-4}	E_a 1st (kJ/mol)	E_a 2nd (kJ/mol)
1	$Cu_{47.5}Zr_{47.5}Al_5$	702	757	991	1183	0.399	0.836	407 ± 10	-
2	$Cu_{47.5}Zr_{47}Al_5Co_{0.5}$	702	754	978	1194	0.397	0.819	385 ± 12	-
3	$Cu_{46.5}Zr_{47.5}Al_5Co_1$	701	753	966	1213	0.393	0.797	355 ± 7	374 ± 9
4	$Cu_{45.5}Zr_{47.5}Al_5Co_2$	700	752	948	1233	0.389	0.769	349 ± 12	-
5	$Cu_{46.5}Zr_{46.5}Al_5Ag_2$	700	758	1043	1163	0.407	0.897	358 ± 13	-
6	$Cu_{46.25}Zr_{46.25}Al_5Ag_2Co_{0.5}$	703	759	1034	1178	0.403	0.878	-	-
7	Cu_{46} $Zr_{46}Al_5Ag_2Co_1$	704	762	1029	1190	0.402	0.865	347 ± 11	-
8	$Cu_{45.5}Zr_{45.5}Al_5Ag_2Co_2$	704	758	1014	1219	0.394	0.832	322 ± 12	388 ± 12
9	$Cu_{45}Zr_{45}Al_5Ag_5$	704	767	< Ts	1139	0.416	1	325 ± 13	-
10	Cu_{45} $Zr_{45}Al_5Ag_5Co_2$	707	764	1067	1203	0.400	0.887	330 ± 9	357 ± 11

Table 4: Mechanical properties for all alloys gained via compression test and ultrasonic measurements, the B2 phase content determined by optical microscopy and DSC and the critical casting diameters. The respective averages and standard deviations are calculated from all measured samples. (* B2 phase content could not be determined due to differing crystallisation sequence between ribbon and rod).

No.	Alloy	R_p (true) (MPa)	ε_p (%)	E_{comp} (GPa)	E_{US} (GPa) ± 0.7	v_{US} ± 0.01	B2 content (vol.%) OM	B2 content (vol.%) DSC ± 0.1	$Ø_{crit}$ (mm)
1	$Cu_{47.5}Zr_{47.5}Al_5$	1710 ± 45	2.2 ± 2.0	87 ± 5	87.5	0.374	0.3 ± 0.7	0.8	≥ 2
2	$Cu_{47.5}Zr_{47}Al_5Co_{0.5}$	1739 ± 50	3.6 ± 1.2	88 ± 2	88.4	0.375	0.6 ± 1.2	0.0	≥ 2
3	$Cu_{46.5}Zr_{47.5}Al_5Co_1$	1722 ± 47	3.0 ± 1.8	89 ± 7	88.4	0.374	1.0 ± 1.0	-*	≥ 2
4	$Cu_{45.5}Zr_{47.5}Al_5Co_2$	1739 ± 15	4.1 ± 2.8	90 ± 2	88.0	0.375	2.1 ± 3.8	12.3	< 2
5	$Cu_{46.5}Zr_{46.5}Al_5Ag_2$	1799 ± 56	2.6 ± 1.5	89 ± 5	88.5	0.374	0.2 ± 0.4	0.0	≥ 2
6	$Cu_{46.25}Zr_{46.25}Al_5Ag_2Co_{0.5}$	1770 ± 28	4.3 ± 3.7	88 ± 4	88.8	0.374	0.4 ± 1.0	-	≥ 2
7	Cu_{46} $Zr_{46}Al_5Ag_2Co_1$	1767 ± 20	2.3 ± 0.7	93 ± 2	88.7	0.374	0.0 ± 0.0	0.0	≥ 2
8	$Cu_{45.5}Zr_{45.5}Al_5Ag_2Co_2$	1869 ± 63	3.1 ± 2.4	91 ± 4	89.7	0.374	2.3 ± 2.5	-*	< 2
9	$Cu_{45}Zr_{45}Al_5Ag_5$	1756 ± 84	1.1 ± 1.2	93 ± 3	90.5	0.374	0.0 ± 0.0	0.0	≥ 2
10	Cu_{45} $Zr_{45}Al_5Ag_5Co_2$	1794 ± 29	2.4 ± 0.7	94 ± 6	90.4	0.373	0.0 ± 0.0	-*	≥ 2

Figures

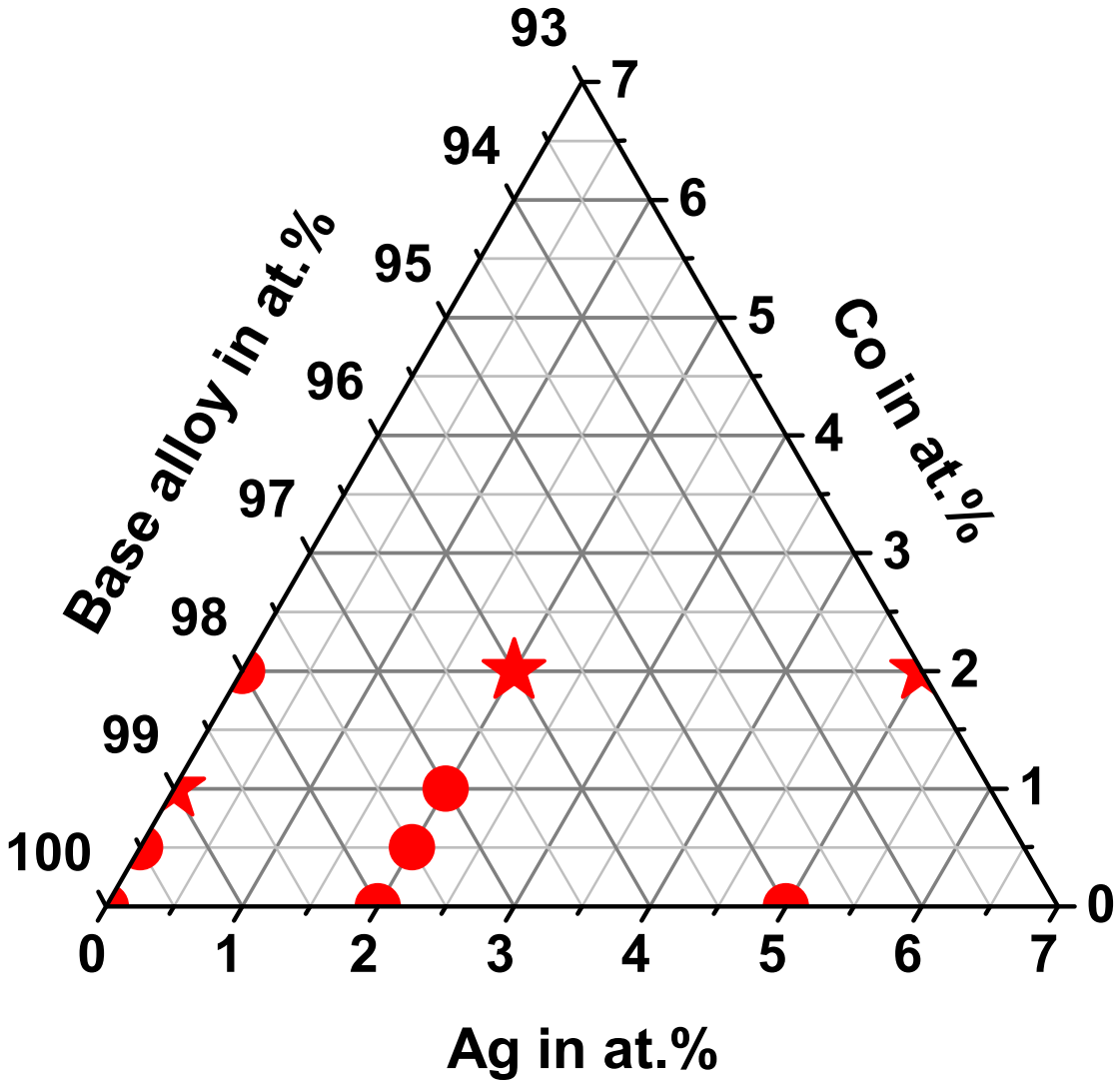

Fig. 1: Section of the pseudo-ternary $Cu_{47.5}Zr_{47.5}Al_5$, Co and Ag phase diagram indicating the investigated compositions. The alloys, in which a metastable “big cube” phase precipitates in the ribbons, are indicated by stars. In the other alloys, $Cu_{10}Zr_7$ and $CuZr_2$ form directly from the glass on heating.

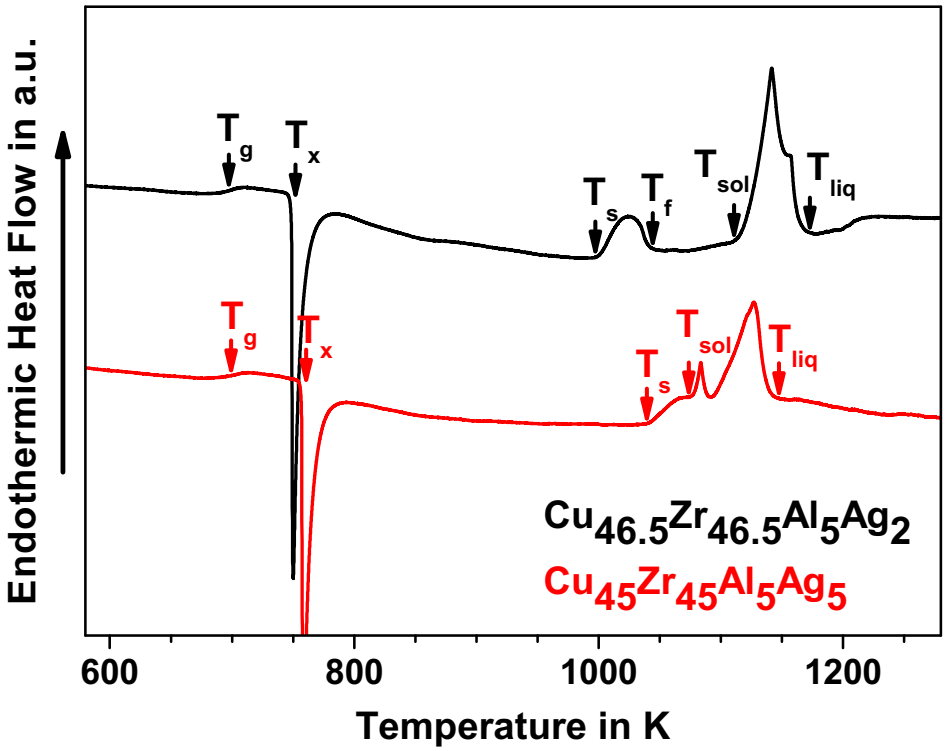

Fig. 2: High-temperature DSC traces (heating rate 20 K/min) for $Cu_{46.5}Zr_{46.5}Al_5Ag_2$ (alloy no. 5) and $Cu_{45}Zr_{45}Al_5Ag_5$ (alloy no. 9) indicating the glass transition temperature (T_g), the crystallization temperature (T_x), the temperature at which the B2 transformation starts (T_s) and finishes (T_f) as well as the solidus (T_{sol}) and liquidus temperature (T_{liq}). T_g and T_x increase, T_{liq} decreases and the eutectoid transformation begins to merge with the melting event when the Ag content is increased. The addition of Ag destabilizes the B2 phase.

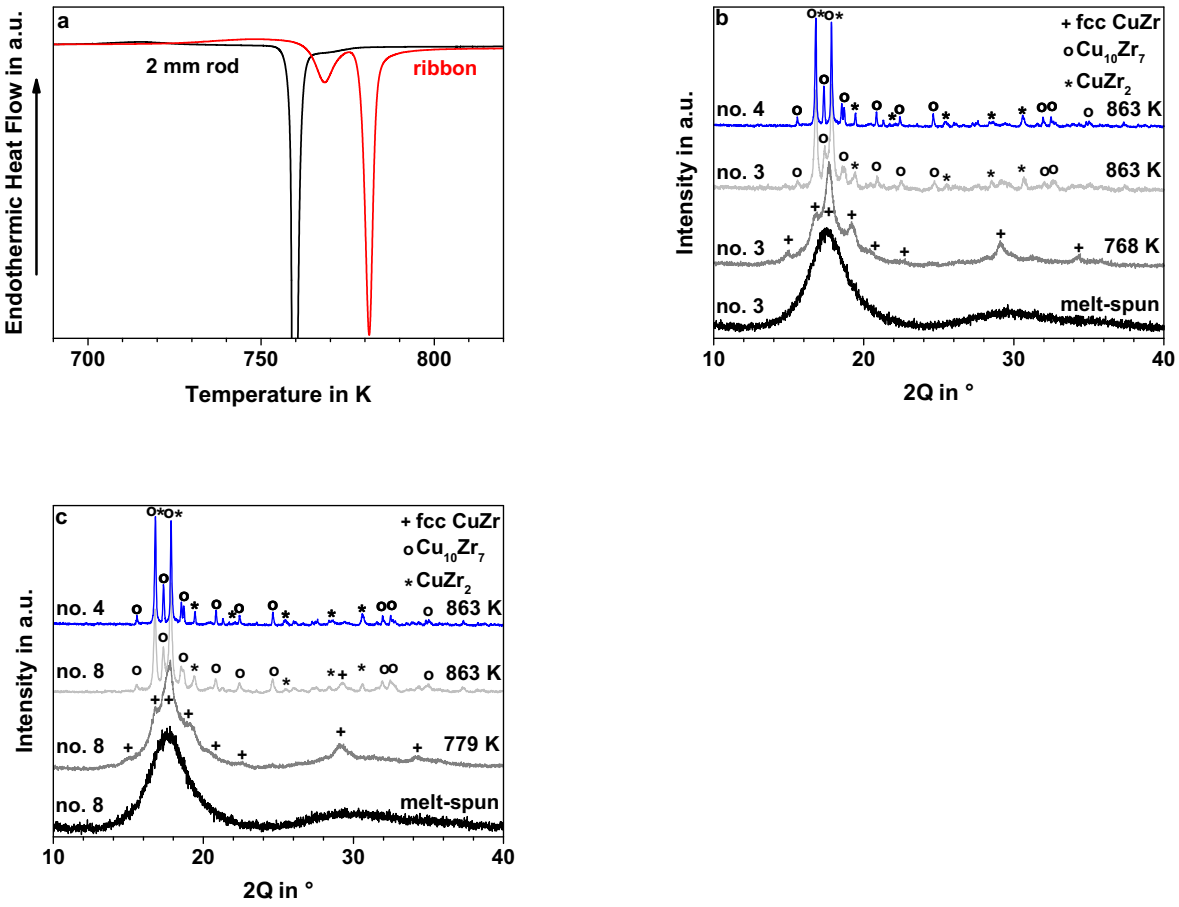

Fig. 3: DSC traces (heating rate 20 K/min) of a $Cu_{45.5}Zr_{45.5}Al_5Ag_2Co_2$ (alloy no. 8) 2 mm rod and ribbon showing the differing crystallization sequence (a). X-ray diffraction patterns of the $Cu_{46.5}Zr_{47.5}Al_5Co_1$ (alloy no. 3) ribbon heated to 768 K (b) and of the $Cu_{45.5}Zr_{45.5}Al_5Ag_2Co_2$ (alloy no. 8) ribbon heated to 863 K (c) (first crystallization event) and to completion of crystallization (863 K). In the latter case, the low-temperature equilibrium phases $Cu_{10}Zr_7$ and $CuZr_2$ form after a metastable “big cube” phase (fcc) has precipitated. For comparison the diffraction pattern of $Cu_{45.5}Zr_{47.5}Al_5Co_2$ (alloy no. 4) after complete crystallization is added.

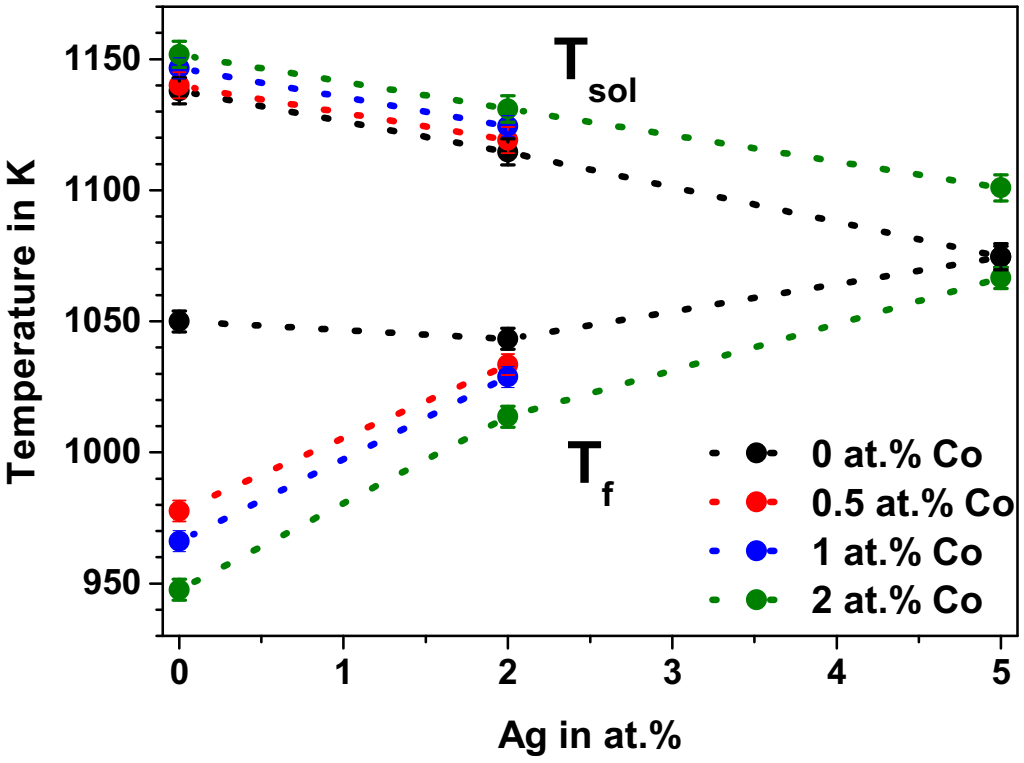

Fig. 4: Solidus temperature (T_{sol}) and B2 transformation finish temperature (T_f) as a function of the Ag and Co content for the rods (as determined from DSC and high temperature DSC runs recorded at 20 K/min heating rate). The higher the Ag content, the smaller the temperature interval (T_{sol} - T_f), in which the B2 phase is stable. At a given Ag content, the addition of Co increases this temperature interval again.

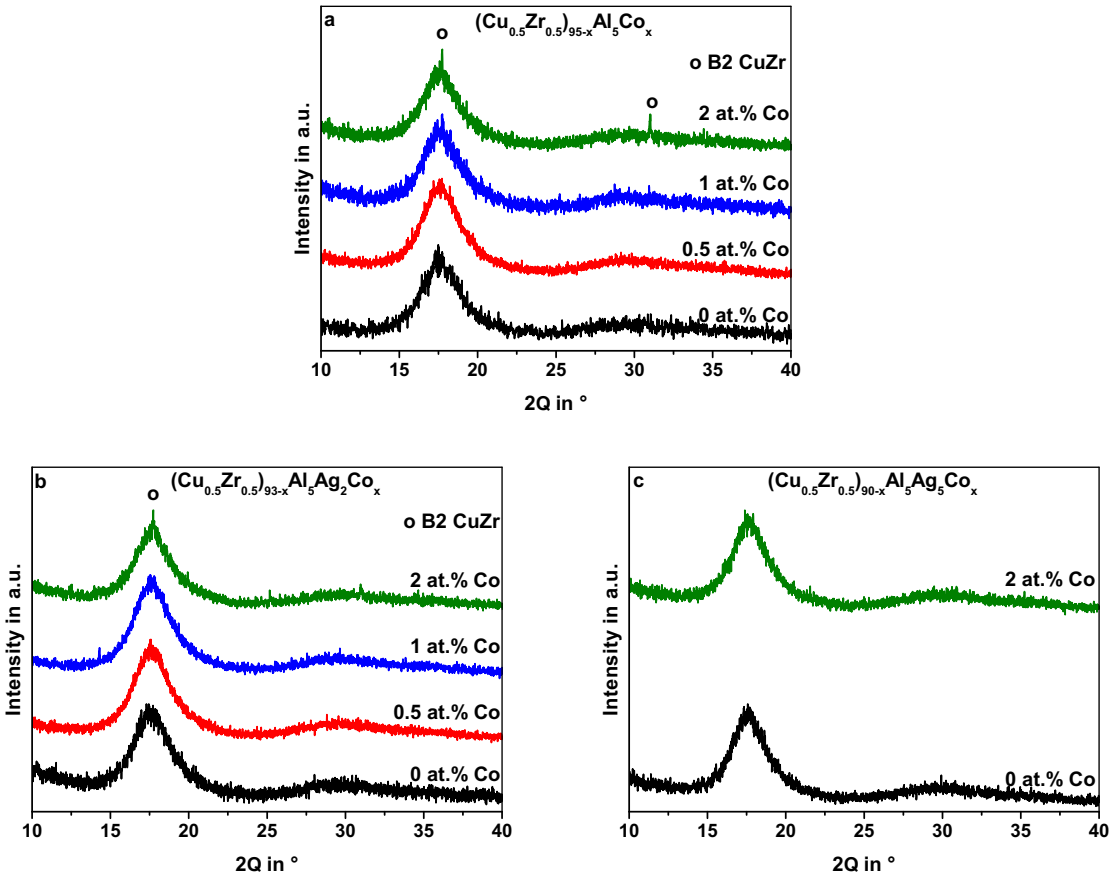

Fig. 5: X-ray diffraction patterns of the rods with a diameter of 2 mm for all alloys. Most of the samples only show the broad diffraction maxima typical of amorphous systems. Only at the largest Co contents (2 at.%) reflections of a B2 (Cu,Co)Zr phase become detectable. The distribution of crystals is heterogeneous and their volume fraction is low (see text) so that it is difficult from these results to correlate glass-forming ability and composition.

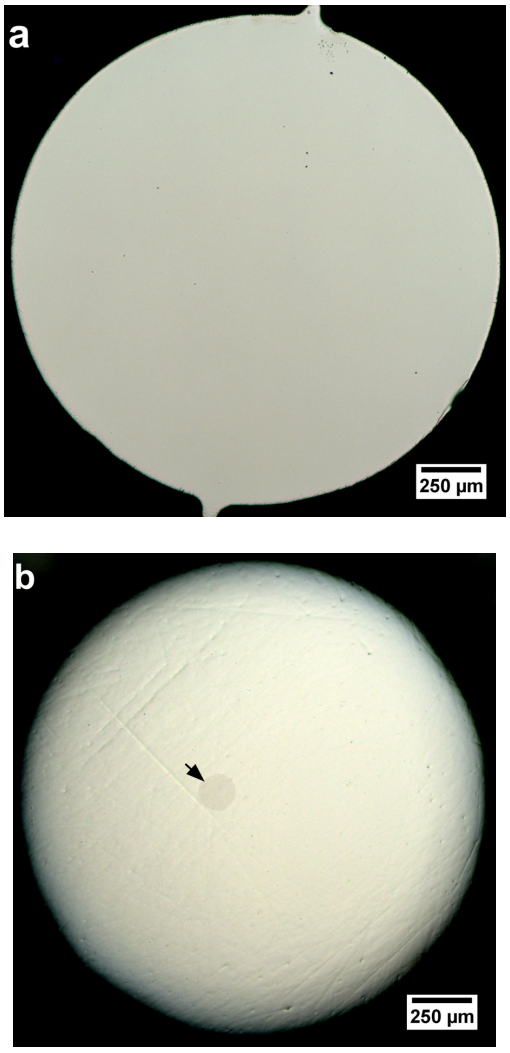

Fig. 6: Optical micrographs of a representative glassy $Cu_{45}Zr_{45}Al_5Ag_5$ sample (alloy no. 9) and a representative $Cu_{45.5}Zr_{47.5}Al_5Co_2$ BMG matrix composite (alloy no. 4). In the latter case, a crystalline particle (~ 150 µm, marked by an arrow) can be found in the featureless glassy matrix. The distribution of these relatively large crystals is heterogeneous over the cross section and the length of the rod.

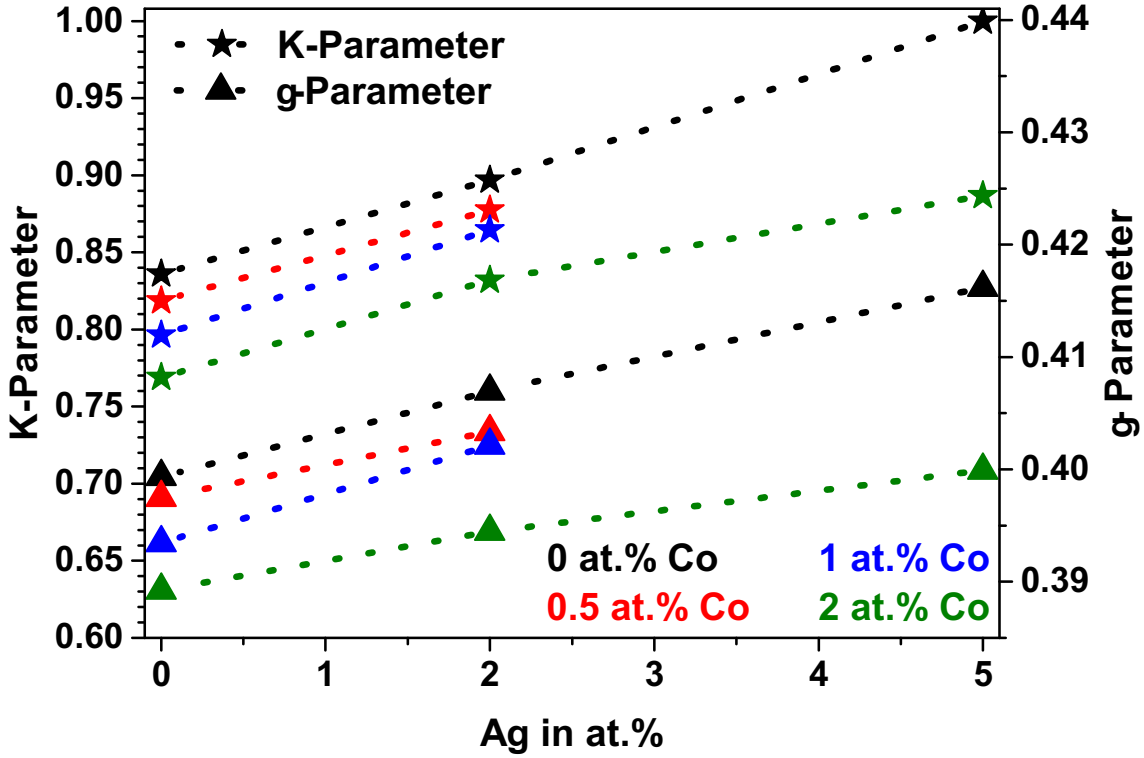

Fig. 7: K- (star) and γ-parameter (triangle) as a function of Ag and Co content of the present rods in order to quantify the tendency of the alloys to solidify into a composite microstructure and to quantify the glass-forming ability of the alloys, respectively. Both parameters follow the same trend and increase with increasing Ag content. The higher the Co content, the lower the K- and γ-parameter, which is associated with the increased stability of the B2 phase.

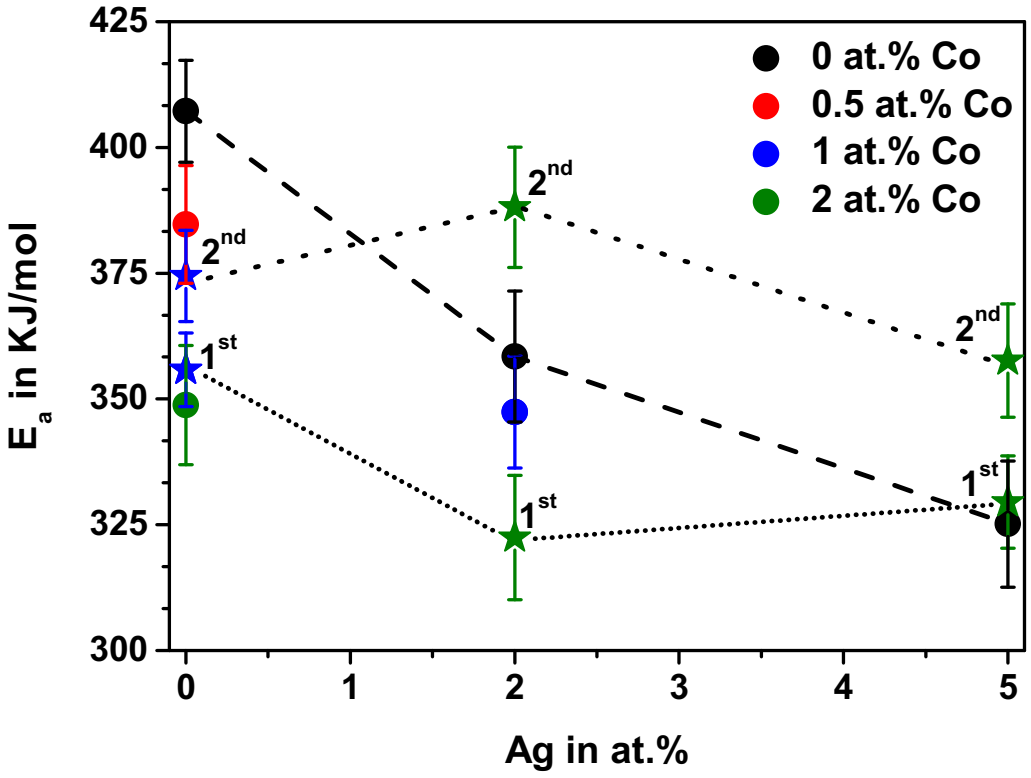

Fig. 8: Activation energy of crystallization as a function of the Ag and Co content for all investigated ribbons. Those samples, which precipitate the “big cube” phase in the first step are marked by stars. Rather than by the crystallization sequence, the activation energy of crystallization is affected by the Ag content. The lines serve as a guide to the eye.

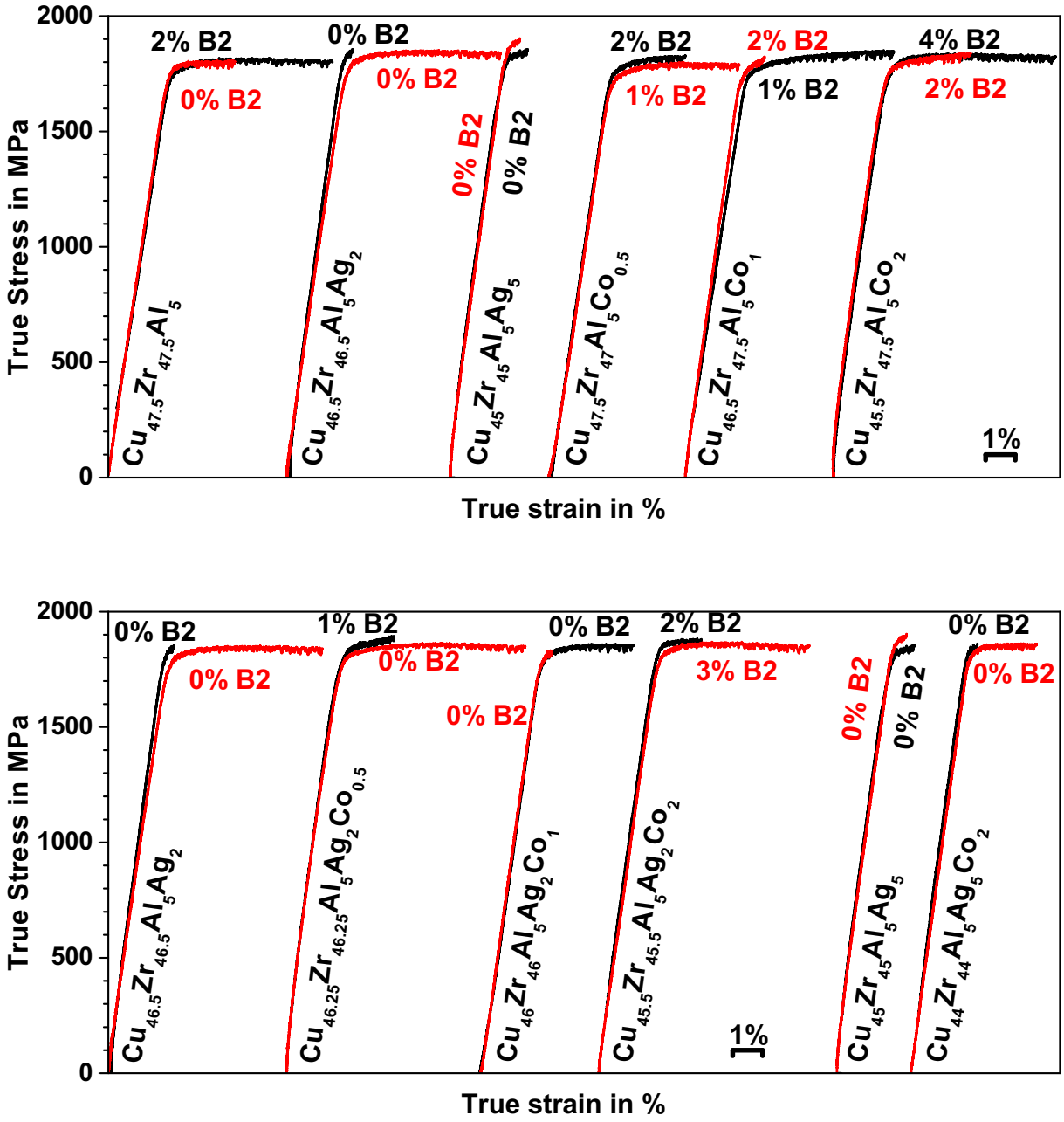

Fig. 9: True stress - true strain curves with the content of B2 phase (OM) displayed for every curve. The curves with the largest and smallest plastic strain are shown for each alloy. They are arranged by incresing Ag or Co contents (a) and increasing Ag and Co contents (with Ag kept constant) (b). Ag decreases the B2 phase content and the plasticity, whereas Co has the reverse effect.